# Accepted Manuscript


*In situ* preparation of reduced graphene oxide/DOPO-based phosphonamidate hybrids towards high-performance epoxy nanocomposites

Wenwen Guo, Bin Yu, Yao Yuan, Lei Song, Yuan Hu

PII: S1359-8368(16)32011-X

DOI: 10.1016/j.compositesb.2017.05.024

Reference: JCOMB 5047

To appear in: *Composites Part B*

Received Date: 20 September 2016

Revised Date: 28 March 2017

Accepted Date: 8 May 2017

Please cite this article as: Guo W, Yu B, Yuan Y, Song L, Hu Y, *In situ* preparation of reduced graphene oxide/DOPO-based phosphonamidate hybrids towards high-performance epoxy nanocomposites, *Composites Part B* (2017), doi: 10.1016/j.compositesb.2017.05.024.

# *In situ* preparation of reduced graphene oxide/DOPO-based phosphonamidate hybrids towards high-performance epoxy nanocomposites

Wenwen Guo,[a, 1] Bin Yu,[a, b, 1] Yao Yuan, [a] Lei Song, *[a] Yuan Hu*[a]

[a] State Key Laboratory of Fire Science, University of Science and Technology of China, 96 Jinzhai Road, Hefei, Anhui 230026, P. R. China

[b] Institute of Textiles & Clothing, Hong Kong Polytechnic University, Hunghom, Kowloon, Hong Kong, P. R. China

* Corresponding authors at: State Key Laboratory of Fire Science, University of Science and Technology of China, Hefei 230026, China (Y. Hu). Tel./fax: +86 551 63601664.

E-mail addresses: leisong@ustc.edu.cn (Lei Song), yuanhu@ustc.edu.cn (Yuan Hu).

[1] These authors contributed equally to this work

**Abstract**

The work reports a strategy based on piperazine-reduced graphene oxide (rGO)/piperazine-based DOPO-phosphonamidate (PiP-DOPO) to overcome the challenge of the dispersion of graphene and mechanical deterioration of epoxy resin (EP) matrix with additive-type flame retardants. Graphene oxide (GO) was functionalized and reduced by piperazine simultaneously, and then incorporated into PiP-DOPO through in situ reaction, resulting in the formation of the hybrids (PD-rGO). Subsequently, the PD-rGO was incorporated into epoxy resin (EP) to fabricate nanocomposite. The structure and thermal properties of PD-rGO were well characterized. The presence of PD-rGO in EP improved the char yields at 700 $^{o}$C and reduced the maximum mass loss rate under nitrogen, indicating the improved thermal stability at elevated temperature. The evaluation of combustion behavior demonstrated that the PHRR and THR values were decreased significantly by 43.0% and 30.2% by the addition of 4 wt% PD-rGO10 (10 wt% rGO in hybrid) in EP respectively, over neat EP. The epoxy composite with 4 wt% PD-rGO5 (5 wt% rGO in hybrid) could pass UL-94 V0 rating and the LOI was 28.0%. The flame retardant mechanism could be attributed to the synergism between two compositions in PD-rGO hybrid: the PiP-DOPO is favorable to flame spread inhibition in UL-94 burning test, while the barrier effect of graphene is dominant in terms of heat release rate suppression. Moreover, the addition of PD-rGO hybrid led to slightly improved storage modulus and tensile strength, due to the high stiffness of graphene. The PD-rGO hybrid combines the outstanding mechanical behavior of graphene with the

good flame retardant effect of DOPO-based compounds, which provides a promising solution to high performance epoxy nanocomposites with improved flame retardant and mechanical properties simultaneously.

**Keywords:** Epoxy resin; Reduced graphene oxide; Hybrids; Mechanical property; Flame retardancy

## 1. Introduction

Epoxy resins (EPs) are one of the well-known thermosetting polymers and have been used in various fields, such as surface coating, adhesives and composites because of their superior physical and chemical properties [1-3]. However, the flammability of EPs limits their application in some areas. Therefore, flame retardant EPs have been attracting increasing attention. Considering the generation of toxic and corrosive gases of the halogenated FRs during combustion, there is a trend toward using halogen-free FRs in EPs.

Phosphorus-containing FRs have been widely developed to achieve the flame retardancy of polymeric materials, due to their high efficiency and less release of toxic gases and smoke, compared with halogenated flame retardants [4-6]. These FRs are versatile as they can exhibit both condensed and/or gas phase flame retardant action [7]. Among various types of phosphorus-containing compounds, 9, 10-dihydro-9, 10-oxa-10-phosphaphenanthrene-10-oxide (DOPO) and its derivatives have attracted extensive attention recently for their notable flame retardant efficiency and versatile reactivity. DOPO-derivatives functions mainly in the gas phase by flame inhibition [8]. To date, various DOPO-derivatives with P-C, P-N and P-O bond

functionality have been developed [9]. A majority of P-C bonded DOPO derivatives, including DOPO-based curing agent [10], reactive co-monomers [11] or non-reactive additives [12], have been applied as flame retardants for EPs. The DOPO derivatives have been proved to be effective to improve the flame retardant behavior of EPs [13,14].

Very recently, P-N bonded DOPO derivatives have been reported to be effective flame retardants for polyurethane foams [9, 15]. For the preparation of DOPO-based phosphoramidates, it is easy to convert the P-H bond of DOPO to a P-N bond by the Atherton-Todd reaction, leading to the formation of desired phosphonamidate derivatives [8]. The DOPO-based phosphonamidates obtained exhibited high thermal stability. However, the application of DOPO-based phosphonamidates in enhancing flame retardancy of EPs is rarely reported. The reported DOPO-based phosphonamidates were mainly additive-type flame retardants. To achieve required flame retardant classification of EP, high loading of additive is usually required, which will deteriorate mechanical properties. Therefore, exploring novel EP systems with improved flame retardancy and mechanical properties simultaneously is desired.

Graphene, a 2-dimensional one-atom thick carbon layer material, has attracted great interest due to its superior electronic, thermal and mechanical properties [16-18]. The attractive properties of graphene make itself promising application in polymer nanocomposites. Recently, graphene has been used as flame retardant additive in polymer nanocomposites [19-21], resulting from its intrinsic fire resistance and layered characteristic. However, the strong van der Waals interactions between

graphene layers make them tend to aggregation, limiting their wider applications. Moreover, the bare graphene is easily burnt out under air atmosphere, which could not act as an effective barrier to prevent the escape of organic volatiles [22]. To solve the issue, chemical modification of graphene with flame retardants is preferred because graphene oxide, the precursor of graphene, possesses large amount of oxygen functional groups (such as epoxy, hydroxyl) on the surface and edge, which provide reactive sites [23,24]. The flame retardant elements on the surface of graphene can not only facilitate the dispersion of graphene but also generate some char layers during combustion [25]. Liao *et al.* [20] prepared DOPO grafted GO with the reduced GO structure (DOPO-rGO). Significant increases in the char yield of 81% and LOI of 30% were achieved with the addition of 10 wt% DOPO-rGO in epoxy, respectively. However, the influence of inorganic/organic ratio in hybrids on the flame retardancy of polymers has been rarely investigated. Also, the previous work has not mentioned the flame retardant behaviors in the industrial burning tests such as UL-94 [20,26,27].

To achieve high-performance EP composites, in this work, DOPO-based phosphonamidates and reduced GO were combined. Piperazine-based DOPO-based phosphonamidate/piperazine-reduced graphene oxide (PD-rGO) hybrids were successfully prepared via an in situ reaction. Then PD-rGO was incorporated into EP to fabricate flame retardant EP nanocomposites. GO was reduced and functionalized in the presence of piperazine. The thermal and mechanical properties, and combustion behavior of EP nanocomposites were investigated by thermogravimetric analysis (TGA), cone calorimeter, and the flame retardant mechanism was discussed.

## 2. Experimental section

### *2.1. Raw materials*

Biphenol A EP was supplied by Hefei Jiangfeng Chemical Industry Co. Ltd. (Anhui, China). DOPO (purity 98%) was obtained from Shandong Mingshan Fine Chemical Industry Co. Ltd. (Shandong, China). Piperazine, tetrahydrofuran(THF), carbon tetrachloride ($CCl_4$), acetone, triethylamine (TEA), graphite powder, potassium permanganate ($KMnO_4$), hydrochloric acid (HCl), sulfuric acid ($H_2SO_4$, 98%), sodium nitrate ($NaNO_3$) and hydrogen peroxide ($H_2O_2$, 30%) were purchased from Sinopharm Chemical Reagent Co. Ltd. (Shanghai, China). THF and TEA were dried over 4 Å molecular sieves before use. Other reagents were used as-received.

### *2.2. Preparation of PiP-DOPO, rGO and PD-rGO*

PiP-DOPO was prepared according to the method described in the prior literature [8], and the synthetic route of PiP-DOPO are presented in Scheme 1a. Graphite oxide was prepared from graphite powder using a modified Hummers' method [28]. GO was modified and reduced by piperazine and the preparation process was as follows. Briefly, 1.0 g of GO was dispersed in 400 ml of deionized water by ultrasonication for 1 h at room temperature. Then, the obtained suspension was introduced into a 1000 ml three-necked flask equipped with a nitrogen inlet, mechanical stirrer and reflux condenser. Subsequently, 3.0 g of piperazine was added to the flask and the reaction was conducted under nitrogen at 100 $^{o}$C for 6 h. After completion of this reaction, the slurry mixture was filtered and thoroughly washed with deionized water and ethyl alcohol to remove the residual reagent. The filtercake was dried under vacuum at

80 °C overnight. The preparation procedure of PD-rGO flame retardant hybrids was illustrated in Scheme 1b. Briefly, the theoretical 5% loading of rGO in the PD-rGO hybrids were prepared as follows. 1.0 g of rGO, 17.57 g of DOPO, 300 ml of THF and 8.21 g of TEA as catalyst were added to a 500 mL three-necked flask equipped with a reflux condenser and dropping funnel under nitrogen by ultrasonication for 1.0 h. The suspension obtained was stirred and cooled to 0 °C by an external ice water bath cooling. Subsequently, carbon tetrachloride (12.51 g) was added dropwise at a rate that the reaction temperature did not exceed 15 °C. After carbon tetrachloride has been added, the reaction was conducted at room temperature for additional 12 h. Finally, the mixture was filtered and washed thoroughly with THF and deionized water to remove residual reagents. The resultant product was dried under reduced pressure at 80 $^{o}$C overnight. The product is designated as PD-rGOX, implying the theoretical X% weight percentage of rGO in the PD-rGO hybrids.

### *2.3. Preparation of flame retardant epoxy resin composites*

The loadings of flame retardant additives in the EP composites are maintained at 4 wt%. Typically, the EP nanocomposite containing 4.0 wt% PD-rGO5 was prepared as follows: 2.0 g of PD-rGO5 was dispersed in 30 ml of acetone by sonication for 0.5 h. Then, the GO suspension as-obtained was mixed with EP (40.0 g), and the blending was stirred, followed by sonication for another 1 h in a three-necked flask. Next, the acetone was completely evaporated off by heating the mixture at 100 $^{o}$C for 12 h, followed by opening the bottleneck of the flask. Afterwards, 8.0 g of DDM was added into the EP/PD-rGO mixture and then poured into a stainless steel mold. This

blending was pre-cured in an oven at 100 $^{o}$C for 2 h and post-cured at 150 $^{o}$C for another 2 h. Other samples were synthesized by the procedure similar to the one described above. The formulations of EP and its composites are listed in Table 1.

### *2.4. Characterizations*

Fourier Transform Infrared Spectroscopy (FTIR) were recorded on a Nicolet 6700 spectrophotometer (Nicolet Instrument Co., USA).

$^{1}$H and $^{31}$P nuclear magnetic resonance (NMR) (400 MHz) spectra were obtained on a Bruker AV400 NMR spectrometer, using dimethylsulfoxide-$d_6$ as solvent.

X-ray photoelectron spectroscopy (XPS) was performed on a VG Escalab Mark II spectrometer (Thermo-VG Scientific Ltd., UK), using Al $K_\alpha$ excitation radiation ($h\upsilon$ = 1486.6 eV).

X-ray diffraction patterns (XRD) of the samples were recorded on an X-ray diffractometer (Rigaku Co., Japan), using a Cu $K_\alpha$ tube and a Ni filter ($\lambda$ = 0.1542 nm) at 40 kV and 20 mA.

Transmission electron microscopy (TEM) analysis was conducted using a JEOL JEM-2100 instrument (JEOL Co., Ltd., Japan) with an acceleration voltage of 200 kV.

UL-94 vertical burning test was performed on a CZF-II horizontal and vertical burning tester (Jiang Ning Analysis Instrument Company, China) according to ASTM D3801-2010. The dimensions of specimens were 127 × 12.7 × 3 mm$^3$.

LOI values were measured using a HC-2 oxygen index meter (Jiang Ning Analysis Instrument Company, China) according to ASTM D2863-2010. The dimensions of samples were 100 × 6.7 × 3 mm$^3$.

TGA measurement was performed on a Q5000 thermal analyzer (TA Co., USA) with a heating rate of 20 $^{o}$C/min.

Combustion performance under forced-flame combustion scenario was evaluated by a cone calorimetry (Fire Testing Technology, UK) under an incident flux of 35 kW/m$^2$ according to ISO 5660. The dimensions of samples were 100 × 100 × 3 mm$^3$.

The micro-scale combustion performance was measured on an MCC-2 micro-scale combustion calorimeter (Fire Testing Technology, UK), according to ASTM D7309-2007 (Method A). About 5 mg of sample were heated up to 650 ºC at a linear heating rate of 1 ºC/s under a nitrogen flow of 80 cm$^3$/min. The volatile and anaerobic thermal degradation products in the nitrogen stream were mixed with a 20 cm$^3$/min $N_2/O_2$ stream (20% $O_2$) prior entering the combustion furnace at 900 ºC. Each sample was run in three replicates.

Dynamic mechanical thermal analysis (DMTA) was measured using a DMA Q800 apparatus (TA Instruments Inc., USA) in bending modes at a heating rate of 5 °C/min. The frequency of dynamic oscillatory loading was 1 Hz.

The tensile tests were carried out on a CMT6104 universal testing system (MTS Systems, China) according to ASTM D3039-08 method, at a crosshead speed of 1.0 mm/min. At least five runs were repeated for each sample and the average value was reported.

Scanning electron microscope (SEM) micrographs of samples were acquired on a FEI Sirion 200 scanning electron microscope at an acceleration voltage of 10 kV.

Raman spectra were obtained on a LabRAM-HR Confocal Raman Microprobe

(JobinYvon Instruments, France) using a 514.5 nm argon ion laser.

## 3. Results and discussion

### *3.1. Characterization of PD-rGO*

Fig. 1a presents the FTIR spectra of GO, rGO, PD-rGO5 and PD-rGO10. The FTIR spectrum of GO shows some typical absorption peaks of oxygen-containing groups: O-H stretching vibration (3400 $cm^{-1}$), C=O stretching vibration (1725 $cm^{-1}$), C=C or $H_2O$ vibration (1620 $cm^{-1}$), C-O-C stretching vibration (1055 $cm^{-1}$) [29]. After the reduction of GO with piperazine, there is a dramatic decrease in the peaks intensity of oxygen functionalities, suggesting the partial reduction of GO. The appearance of new peaks at 2923 and 2855 $cm^{-1}$, 1565 $cm^{-1}$ are attributed to C-H and C-N vibrations, respectively. These results indicate that GO have been successfully functionalized and reduced. The FTIR spectrum of PiP-DOPO reveals some characteristic peaks at 3060, 2966, 2856, 1596, 1207, 972 and 755 $cm^{-1}$, which is in accordance with the prior report [15]. The FTIR spectra of PD-rGO5 and PD-rGO5 are similar to that of PiP-DOPO, indicating the formation of PiP-DOPO/rGO hybrids.

The chemical structure of PiP-DOPO and its hybrids are further confirmed by the $^{1}H$ and $^{31}P$ NMR spectra. In the $^{1}H$ NMR spectrum of PiP-DOPO (Fig. 1b), the resonance peak at 3.13 ppm is attributed to the protons of -$CH_2$-. In addition, the resonance peaks in the range of 7.10-8.50 ppm are corresponding to the aromatic protons in DOPO structures. In the $^{31}P$ NMR spectra (Fig. 1c), PiP-DOPO and its hybrids present a single sharp resonance peak at 14.1 ppm, indicating the formation of PD-rGO hybrids.

Fig. 1d shows the XRD patterns of GO, rGO, PiP-DOPO and its hybrids. The characteristic diffraction peak of GO is located at 2θ = 10.5°, corresponding to the (002) reflection of GO [30]. The weak peak at 2θ ~ 42º is ascribed to the (100) reflection of GO. Upon chemical modification of GO with piperazine, rGO exhibits a diffraction peak at a smaller diffraction angle of 9.5°, suggesting a significant enlargement in interlayer spacing. This is attributed to the intercalation of piperazine into GO via ring-opening reaction. No visible diffraction peak is observed in the XRD patterns in the range of 3-10$^{o}$, indicating that the rGO sheets are exfoliated or dispersed disorderly in the flame retardant via in situ reaction

The structures of GO, rGO, PD-rGO5 and PD-rGO10 were investigated by XPS, as shown in Fig. 2. The element content of GO, RGO, PD-rGO5 and PD-rGO10 measured from XPS analysis is listed in Table 2. GO (Fig. 2a) has a considerable degree of oxidation with a C/O atomic ratio of 67.9%/30.6%. rGO exhibits increased intensity in $N_{1s}$ peak relative to GO, while PD-rGO5 and PD-rGO10 exhibits increased intensity in $P_{2s}$ and $P_{2p}$ peaks relative to rGO. The increase in the intensity of $N_{1s}$ peak is attributed to the doping of nitrogen into graphene lattice during the reduction and modification reaction [31]. The appearance of $P_{2s}$ and $P_{2p}$ peaks is originating from the wrapped PiP-DOPO on the surface of rGO. From Fig. 2b, it can be observed that the $C_{1s}$ XPS spectrum of GO is deconvoluted into four types of carbon, including C-C (284.6 eV), C-O (286.6 eV), C=O (287.8 eV) and C(O)OH (288.9 eV) [32]. After the reduction reaction, the $C_{1s}$ spectrum of rGO (Fig. 2c) exhibits significant decrease in the relative peak areas of these oxygen-containing

groups, indicating that most of the oxygen functional groups have been successfully removed. Moreover, a new peak at 285.6 eV corresponding to C-N bond [33], is also observed in the spectrum of rGO. In the case of PD-rGO, C-C at 284.8 eV and C-N & C-O-P at 286.1 eV are observed in the $C_{1s}$ spectrum (Fig. 2d) [23]. These results demonstrate that GO has been reduced and functionalized, and formation of flame retardant hybrids.

The morphological features for GO and rGO are directly observed by TEM. Fig. 3a reveals that GO presents transparent and thin two-dimensional nanosheets. The apparent wrinkles and ripples on the GO are due to the extreme thinness of the nanosheets. After reduction, more wrinkles and ripples on the surface are observed for rGO (Fig. 3b).

SEM images of the fracture surface provide the information concerning the interfacial interactions between the matrix and graphene sheets. Relatively smooth fractured surfaces are observed for the pure EP (Fig. 4a), due to the typical fracture behavior of homogeneous material. However, the fractured surfaces of EP composites are much rougher than those of EP (Fig. 4b-d). The SEM image of EP/PiP-DOPO (Fig. 4b) is similar to that of EP/PD-rGO5 without obvious agglomeration of additives on the surfaces. It should be noted that no apparent graphene sheets are distributed on the surface for EP/PD-rGO5 (Fig. 4c). This is probably due to the reason that graphene sheets are wrapped by PiP-DOPO through in situ reaction. As the content of graphene in PiP-DOPO increases, graphene sheets are embedded into the matrix without pulling out. These results indicate that the rGO is well-dispersed in the matrix, as well as

forming superior interfacial adhesion with the matrix.

Fig. 5 presents the (a) TG and (b) DTG curves of GO, rGO, PiP-DOPO, PD-rGO5 and PD-rGO10 under nitrogen. The initial degradation temperature is defined as the temperature at 5 wt% mass loss ($T_{-0.05}$). The temperature of maximum weight-loss rate ($T_{max}$) is obtained from the peak maxima of DTG curves. It is observed that GO starts to lose weight below 100 °C due to evaporation of water molecules held in the samples [34]. The mass loss over 150 °C is attributable to the decomposition of oxygen-containing groups. The char residues at 800 $^{o}$C are approximately 44.1 wt%. Reduced by piperazine, rGO is more stable than GO, exhibiting higher thermal stability and char residues (65.0%). PiP-DOPO exhibits a high $T_{-0.05}$ of 304 $^{o}$C and low char residues of around 3.5%. After the incorporation of rGO, the thermal stability of PD-rGO is lowered, due to the lower thermal stability of rGO. However, the residual char for PD-rGO5 and PD-rGO10 at 800 $^{o}$C are remarkably increased, which are 9.5% and 13.1%, respectively. DTG curves reveal that the presence of rGO decreases the degradation rate of PiP-DOPO, due to the barrier effect of graphene sheets.

### *3.2. Thermal properties and flame retardancy*

Fig. 6 shows the TG and DTG curves of EP and its composites under nitrogen and air atmosphere, and the corresponding data are listed in Table 3. Under nitrogen atmosphere, neat EP undergoes one-stage thermal degradation process in the temperature range of 350-450 $^{o}$C, which is attributed to the degradation of principal EP networks. The $T_{-0.05}$ and $T_{max}$ of neat EP are 360 and 378 $^{o}$C, respectively, and the

char yield at 700 $^{o}$C is 13.6 wt%. EP composites show similar one-stage degradation behaviors to the control EP. The $T_{0.05}$ and $T_{max}$ of EP composites shift to lower temperature compared to those of pure EP, due to the earlier decomposition of the flame retardant additives. Generally, the earlier degradation of the phosphorus-containing additives could catalyze the degradation of polymers to form the protective char. The char could shield polymers from flame in the early stage of ignition; thereby, the lowered $T_{-0.05}$ and $T_{max}$ is likely necessary rather than a defect of the EP composites [35]. Moreover, the flame retardant additives have little influence on the char yield at 700 $^{o}$C. From Fig. 6b, it can be seen that the addition of PiP-DOPO increases the mass loss rates of EP, while the presence of rGO slightly reduces the value, probably due to the barrier effect of graphene.

The thermal degradation of EP and its composites under air behaves differently from that under nitrogen. In the case of neat EP, its thermal degradation process could be mainly divided into two stages: the first stage locates the temperature range of 360 −480 $^{o}$C corresponding to the scission of the cured epoxy networks, while the second one in the temperature range of 500−650 ° C can be ascribed to the thermal oxidative degradation of the char. In contrast, the thermal degradation process of EP composites displays the similar two-stage behavior as the neat one, excepting the lower $T_{-0.05}$ and $T_{max}$. This finding is similar to the phenomenon under nitrogen. Furthermore, from DTG curve, it can be seen that the maximum mass loss rate the EP composites is higher than that of the neat epoxy, meaning that the addition of PiP-DOPO and PD-rGO could catalyze the thermal degradation of epoxy matrix.

The flame retardancy of EP and its composites was evaluated by UL-94 and LOI measurements, and the results are presented in Table 1. Pure EP displays no rating (NR) in the UL-94 vertical burning test and shows a low LOI value of 22.0%. The addition of PiP-DOPO and PD-rGO imparts significant flame retardant effect to EP: with the loading of 4 wt% PiP-DOPO, its EP composite shows V-1 rating and its LOI value is increased to 27.5%. At the equivalent loading, the EP/PD-rGO5 could pass the UL-94 V-0 rating while the EP/PD-rGO10 only passes the UL-94 V-1 rating, indicating the superior flame retardant efficiency of PD-rGO5 over PD-rGO10. The LOI values of both the EP/PD-rGO5 and the EP/PD-rGO10 are beyond 28.0%. In general, polymeric materials with LOI value greater than 26% are regarded to be difficult to be ignited [36]. The LOI results imply that PD-rGO imparts good flame retardant effect to EP composites.

The combustion behavior of epoxy and its composites was assessed by micro-scale combustion calorimetry (MCC) experiments. The relevant parameters obtained from the MCC include peak heat release rate (PHRR), total heat released (THR), and temperature at PHRR ($T_{PHRR}$), as listed in Table 4. Fig. 7 displays the heat release rate versus temperature plots of epoxy and its composites. The HRR curve for the pure epoxy resin shows a sharp peak, and the associated PHRR and THR are 322 W/g and 28.1 kJ/g, respectively. After incorporating PiP-DOPO into epoxy, the PHRR and THR are reduced by 20% and 14%, respectively. A further reduction in PHRR and THR is achieved by the incorporation of PD-rGO5 in comparison with the sample containing PiP-DOPO. The maximum reduction in PHRR (51%) and THR (26%) is

achieved by incorporation of PD-rGO10 into the epoxy matrix. The $T_{PHRR}$ of the epoxy composites shifts to lower temperature due to the earlier degradation of flame retardant additives, which is in accordance with the TGA experiments aforementioned.

The fire behavior of the samples was further studied by the cone calorimeter, which can provide various fire-related parameters including time to ignition (TTI), PHRR, THR, smoke produce rate (SPR), and time to PHRR. Fig. 8 presents the (a) HRR and (b) THR versus time curves of EP and its composites, and the related data are summarized in Table 5. Fig. 8a reveals that the pure EP burns very rapidly after ignition and the PHRR is as high as 1736 kW/m$^2$. With the addition of 4 wt% PiP-DOPO, the PHRR of EP/PiP-DOPO is decreased significantly to 1159 kW/m$^2$. At the same loading, the PHRR of EP/PD-rGO5 is further reduced to 1050 kW/m$^2$. Among the flame retardant samples, EP/PD-rGO10 exhibits the lowest PHRR. The PHRR values for EP/PiP-DOPO, EP/PD-rGO5 and EP/PD-rGO10 are reduced by 33.2%, 39.5% and 52.6% relative to that of pure EP, respectively. Similar to HRR curves, the EP/PD-rGO10 exhibits considerably reduced THR (47.4% reduction), which is lower than those of EP/PD-rGO5 and EP/PiP-DOPO. The significant reduction of PHRR and THR for EP/PD-rGO10 is attributed to the insulating barrier function of a cohesive and compact char layer during combustion, delaying and reducing the permeation of oxygen and the escape of volatile degradation products.

From Table 5, it can be seen that addition of flame retardant additives results in a slightly reduced TTI. As mentioned in TGA results, the earlier degradation of flame

retardant additives catalyzes the epoxy matrix to form the protective char, which is responsible for the lowered TTI. The SPR is also decreased after the addition of PD-rGO hybrids, indicating that PiP-DOPO or PD-rGO acts as a smoke suppressant during combustion. The fire growth rate index (FIGRA) is calculated from the ratio of PHRR/time to PHRR [35]. All the EP composites show reduced FIGRA in contrast to pure EP. The FIGRA value is decreased dramatically from 31.9 kW/($m^2$·s) for neat EP to 15.5 kW/($m^2$·s) for EP/PD-rGO10, a 51% reduction in FIGRA relative to neat EP, implying the significantly enhanced flame retardancy of the material.

### *3.3. Mechanical property*

The viscoelastic properties of cured epoxy and its composites were evaluated by dynamic mechanical thermal analysis. Fig. 9 presents the (a) storage modulus and (b) Tan δ curves of EP and its composites as a function of temperature. All the samples show the typical viscoelastic behaviors of thermosetting polymers, from glassy plateau, transition region to rubbery plateau. It can be seen that the storage modulus of EP/PD-rGO composites at both the glassy and the rubbery plateau is slightly higher than that of neat EP, demonstrating that addition of the PD-rGO hybrids induces a favorable impact on the storage modulus of the epoxy composites. Generally, the storage modulus for the polymer composites is dependent strongly on the inorganic phase, the interfacial interaction and the cross-linking density of the polymer matrix [37]. The slightly enhanced storage modulus could presumably be attributed to the high specific surface area and high stiffness of graphene. The glass transition temperature ($T_g$) is determined from the peak of Tan δ ~ T curve. Pure EP displays a

$T_g$ of 174 $^oC$, while the $T_g$ of EP/PiP-DOPO, EP/PD-rGO5 and EP/PD-rGO10 composite is 173, 175 and 171 $^oC$, respectively. The change in $T_g$ is really negligible, which indicates that no interactions between the modified nanofiller and the epoxy matrix occur in the systems investigated.

Static tensile loading tests were also measured to assess the effect of flame retardant additives on the tensile properties of EP composites. The tensile strength, elongation at break and tensile modulus are listed in Table 6. Tensile modulus increases after incorporating PD-rGO hybrids into epoxy. An increase of 7% for EP/ PD-rGO5, 11% for EP/PD-rGO10, at a 4 wt% content level, is observed. The enhanced modulus can be directly ascribed to the stiffening effect of PD-rGO hybrids since the graphene has a much higher modulus than epoxy. This finding is consistent with the storage modulus results. Neat EP shows a tensile strength of 50.6 MPa and a low elongation at break of 2.6%, indicating a relatively brittle material. There are no significant change in the tensile strength and elongation at break for epoxy composites containing flame retardant additives. The PiP-DOPO and PD-rGO hybrid used in this work do not lead to the deteriorated mechanical properties of epoxy matrix, and the good mechanical behaviors are retained simultaneously with improved flame retardancy.

### *3.4. Char residue analysis*

Fig. 10 shows the SEM images of the residual char: (a) EP, (b) EP/PiP-DOPO, (c) EP/PD-rGO5 and (d) EP/PD-rGO10 after cone calorimeter tests. The char from pure EP displays a discontinuous and loose morphology, and some cracks are clearly

observed on the surface. Compared to neat EP, the EP/PiP-DOPO presents large holes, probably due to the rapid release of degradation products in a short time, which is consistent with the DTG analysis. The char layer of EP/PD-rGO5 is more compact than that of EP/PiP-DOPO and only few cracks appear on the surface. Further increasing the loading of rGO in PD-rGO leads to the formation of more tight and thick frame-work on the surface of the char. The reason for this phenomenon is due to relatively slow release of volatile gases during thermal degradation and the higher charring ability. The char layer with compact structure reduces the mass and energy transfer, thus retarding the degradation of the underlying materials.

Raman spectroscopy was used to characterize the structure of carbonaceous materials. Fig. 11 presents the Raman spectra of the char residues of EP and its composites after cone calorimeter tests. The spectrum of control EP presents two prominent peaks at approximately 1367 and 1595 $cm^{-1}$, corresponding to D and G band, respectively. The ratio of the integrated intensities of D to G band ($I_D/I_G$) is used to estimate the graphitization degree of the residual char. The $I_D/I_G$ value of the char for EP is 2.80. The addition of PD-rGO decreases the $I_D/I_G$ value of the EP composites, while PiP-DOPO improves the value. Graphene as micro-char is the main contributor for the formation of graphitized carbons. The more graphitized carbons of the char structure imply higher thermal stability. The char layer with high thermal stability can act as a barrier to prevent the escape of organic volatiles, and decrease the heat release rate during combustion.

**4. Conclusions**

In this work, DOPO-based phosphonamidate/reduced GO hybrids (PD-rGO) were successfully prepared via in situ reaction. Then PD-rGO was incorporated into epoxy to fabricate flame retardant composites. The incorporation of PD-rGO hybrid reduced the thermal stability under both nitrogen and air atmosphere which was ascribed to that the earlier decomposition of the flame retardant additives could catalyze the degradation of polymers to form the protective char. The presence of 4 wt% PD-rGO10 significantly reduced the PHRR and THR values by 43.0% and 30.2%, respectively, compared to neat EP. The addition of 4 wt% PD-rGO5 into EP achieved UL-94 V0 rating and the LOI was 28.0%. These findings implied the synergistic interaction between two compositions in PD-rGO hybrid: the DOPO-based phosphonamidate was more effective in inhibiting the flame spread to meet the industrial requirement, while the graphene served as physical barrier for lowering the heat release rate during combustion. In addition to the remarkable flame retardant enhancement, the storage modulus, elastic modulus and tensile strength of EP/PD-rGO composites were slightly increased as well, due to the high stiffness of graphene species. The functionalization of graphene with flame retardants provides superior solution over traditional methods in terms of flame retardant and mechanical enhancements simultaneously.

**Acknowledgments**

The work was financially supported by National Basic Research Program of China (973 Program) (No. 2014CB931804), National Natural Science Foundation of China (No. 21374111) and Fundamental Research Funds for the Central Universities

(No. WK2320000032).

**References**

[1] Zotti A, Borriello A, Ricciardi M, Antonucci V, Giordano M, Zarrelli M. Effects of sepiolite clay on degradation and fire behaviour of a bisphenol A-based epoxy. Compos Part B-Eng 2015;73:139-48.

[2] Guan FL, Gui CX, Zhang HB, Jiang ZG, Jiang Y, Yu ZZ. Enhanced thermal conductivity and satisfactory flame retardancy of epoxy/alumina composites by combination with graphene nanoplatelets and magnesium hydroxide. Compos Part B-Eng 2016;98:134-40.

[3] Oliwa R, Heneczkowski M, Oleksy M, Galina H. Epoxy composites of reduced flammability. Compos Part B-Eng 2016;95:1-8.

[4] Lu SY, Hamerton I. Recent developments in the chemistry of halogen-free flame retardant polymers. Prog Polym Sci 2002;27:1661-712.

[5] Levchik SV, Weil ED. A review of recent progress in phosphorus-based flame retardants. J Fire Sci 2006;24:345-64.

[6] Chen L, Wang YZ. A review on flame retardant technology in China. Part I: development of flame retardants. Polym Adv Technol 2010;21:1-26.

[7] Green J. A review of phosphorus-containing flame retardants. J Fire Sci 1992;10:470-87.

[8] Neisius NM, Lutz M, Rentsch D, Hemberger P, Gaan S. Synthesis of DOPO-based phosphonamidates and their thermal properties. Ind Eng Chem Res 2014;53:2889-96.

[9] Salmeia KA, Gaan S. An overview of some recent advances in DOPO-derivatives:

Chemistry and flame retardant applications. Polym Degrad Stabil 2015;113:119-34.

[10] Lin CH, Cai SX, Lin CH. Flame-retardant epoxy resins with high glass-transition temperatures. II. Using a novel hexafunctional curing agent: 9, 10-dihydro-9-oxa-10-phosphaphenanthrene 10-yl-tris (4-aminophenyl) methane. J Polym Sci Part A: Polym Chem 2005;43:5971-86.

[11] Liu YL. Epoxy resins from novel monomers with a bis-(9, 10-dihydro-9-oxa-10-oxide-10-phosphaphenanthrene-10-yl-) substituent. J Polym Sci Part A: Polym Chem 2002;40:359-68.

[12] Wang X, Song L, Xing W, Lu H, Hu Y. A effective flame retardant for epoxy resins based on poly (DOPO substituted dihydroxyl phenyl pentaerythritol diphosphonate). Mater Chem Phys 2011;125:536-41.

[13] Perret B, Schartel B, Stoss K, Ciesielski M, Diederichs J, Doring M, et al. Novel DOPO-based flame retardants in high-performance carbon fibre epoxy composites for aviation. Eur Polym J 2011;47:1081-9.

[14] Lin CH, Wu CY, Wang CS. Synthesis and properties of phosphorus-containing advanced epoxy resins. II. J Appl Polym Sci 2000;78:228-35.

[15] Gaan S, Liang S, Mispreuve H, Perler H, Naescher R, Neisius M. Flame retardant flexible polyurethane foams from novel DOPO-phosphonamidate additives. Polym Degrad Stabil 2015;113:180-8.

[16] Chandra Y, Scarpa F, Adhikari S, Zhang J, Flores EIS, Peng HX. Pullout strength of graphene and carbon nanotube/epoxy composites. Compos Part B-Eng 2016;102:1-8.

[17] Shiu SC, Tsai JL. Characterizing thermal and mechanical properties of graphene/epoxy nanocomposites. Compos Part B-Eng 2014;56:691-7.

[18] Tang GQ, Jiang ZG, Li XF, Zhang HB, Hong S, Yu ZZ. Electrically conductive rubbery epoxy/diamine-functionalized graphene nanocomposites with improved mechanical properties. Compos Part B-Eng 2014;67:564-70.

[19] Huang G, Gao J, Wang X, Liang H, Ge C. How can graphene reduce the flammability of polymer nanocomposites? Mater Lett 2012;66:187-9.

[20] Liao SH, Liu PL, Hsiao MC, Teng CC, Wang CA, Ger MD, et al. One-step reduction and functionalization of graphene oxide with phosphorus-based compound to produce flame-retardant epoxy nanocomposite. Ind Eng Chem Res 2012;51:4573-81.

[21] Qian XD, Song L, Yu B, Wang B, Yuan B, Shi Y, et al. Novel organic–inorganic flame retardants containing exfoliated graphene: Preparation and their performance on the flame retardancy of epoxy resins. J Mater Chem A 2013;1:6822-30.

[22] Yu B, Shi Y, Yuan B, Qiu S, Xing W, Hu W, et al. Enhanced thermal and flame retardant properties of flame-retardant-wrapped graphene/epoxy resin nanocomposites. J Mater Chem A 2015;3:8034-44.

[23] Hsiao MC, Liao SH, Lin YF, Wang CA, Pu NW, Tsai HM, et al. Preparation and characterization of polypropylene-graft-thermally reduced graphite oxide with an improved compatibility with polypropylene-based nanocomposite. Nanoscale 2011;3:1516-22.

[24] Allen MJ, Tung VC, Kaner RB. Honeycomb carbon: A review of graphene. Chem

Rev 2009;110:132-45.

[25] Qian XD, Yu B, Bao C, Song L, Wang B, Xing W, et al. Silicon nanoparticle decorated graphene composites: Preparation and their reinforcement on the fire safety and mechanical properties of polyurea. J Mater Chem A 2013;1:9827-36.

[26] Liu Y, Babu HV, Zhao JQ, Goni-Urtiaga A, Sainz R, Ferritto R, et al. Effect of Cu-doped graphene on the flammability and thermal properties of epoxy composites. Compos Part B-Eng 2016;89:108-16.

[27] Wang ZH, Wei P, Qian Y, Liu JP. The synthesis of a novel graphene-based inorganic-organic hybrid flame retardant and its application in epoxy resin. Compos Part B-Eng 2014;60:341-9.

[28] Hummers Jr WS, Offeman RE. Preparation of graphitic oxide. J Am Chem Soc 1958;80:1339.

[29] Stankovich S, Piner RD, Nguyen ST, Ruoff RS. Synthesis and exfoliation of isocyanate-treated graphene oxide nanoplatelets. Carbon 2006;44:3342-7.

[30] Zhao FG, Li WS. Dendronized graphenes: Remarkable dendrimer size effect on solvent dispersity and bulk electrical conductivity. J Mater Chem 2012;22:3082-7.

[31] Wu J, Zhang D, Wang Y, Hou B. Electrocatalytic activity of nitrogen-doped graphene synthesized via a one-pot hydrothermal process towards oxygen reduction reaction. J Power Sources 2013;227:185-90.

[32] Zhang C, Hao R, Liao H, Hou Y. Synthesis of amino-functionalized graphene as metal-free catalyst and exploration of the roles of various nitrogen states in oxygen reduction reaction. Nano Energy 2013;2:88-97.

[33] Montmeat P, Veignal F, Methivier C, Pradier CM, Hairault L. Study of calixarenes thin films as chemical sensors for the detection of explosives. Appl Surf Sci 2014;292:137-41.

[34] Park S, An J, Potts JR, Velamakanni A, Murali S, Ruoff RS. Hydrazine-reduction of graphite-and graphene oxide. Carbon 2011;49:3019-23.

[35] Wang X, Kalali EN, Wang DY. Renewable cardanol-based surfactant modified layered double hydroxide as a flame retardant for epoxy resin. ACS Sustain Chem Eng 2015;3:3281-90.

[36] Pan LL, Li GY, Su YC, Lian JS. Fire retardant mechanism analysis between ammonium polyphosphate and triphenyl phosphate in unsaturated polyester resin. Polym Degrad Stabil 2012;97:1801-6.

[37] Zhou SX, Wu LM. Phase separation and properties of UV-curable polyurethane/zirconia nanocomposite coatings. Macromol Chem Phys 2008;209:1170-81.

**Captions**

**Table 1** Formulations and flame retardancy of EP and its composites

**Table 2** Element content of GO, RGO, PD-rGO5 and PD-rGO10 measured from XPS analysis

**Table 3** TGA data of EP and its composites

**Table 4** MCC data of neat EP and its composites

**Table 5** Cone calorimeter data of neat EP and its composites

**Table 6** Tensile properties of neat EP and its composites

**Scheme 1** Preparation of (a) PiP-DOPO and (b) PD-rGO

**Fig. 1** (a) FTIR spectra of GO, rGO, PD-rGO5 and PD-rGO10; (b) $^{1}H$ and (c) $^{31}P$ NMR spectra of PiP-DOPO and its hybrids; (d) XRD patterns of GO, rGO, PiP-DOPO and PD-rGO hybrids.

**Fig. 2** (a) XPS spectra of GO, rGO, PD-rGO5 and PD-rGO10; High resolution $C_{1s}$ XPS spectra of (b) GO, (c) rGO and (d) PD-rGO

**Fig. 3** TEM images of (a) GO and (b) rGO

**Fig. 4** SEM images of the fracture surface of (a) pure EP, (b) EP/PiP-DOPO, (c) EP/PD-rGO5 and (d) EP/PD-rGO10

**Fig. 5** (a) TG and (b) DTG curves of GO, rGO, PiP-DOPO, PD-rGO5 and PD-rGO10 under nitrogen

**Fig. 6** TG curves of EP and its composites under (a) nitrogen and (b) air; DTG curves of EP and its composites under (c) nitrogen and (d) air

**Fig. 7** HRR vs. temperature curves of EP and its composites obtained from MCC

**Fig. 8** (a) HRR and (b) THR vs. time curves of EP and its composites obtained from cone calorimetry

**Fig. 9** (a) Storage modulus and (b) Tan δ curves of EP and its composites as a function of temperature

**Fig. 10** SEM images of the residual char: (a) EP, (b) EP/PiP-DOPO, (c) EP/PD-rGO5 and (d) EP/PD-rGO10 after cone calorimeter tests

**Fig. 11** Raman spectra of the char residues of EP and its composites

**Table 1**

| Sample | PiP-DOPO (wt%) | PD-rGO5 (wt%) | PD-rGO10 (wt%) | LOI (%) | UL-94 |
|---|---|---|---|---|---|
| EP | - | - | - | 22.0 | NR |
| EP/PiP-DOPO | 4 | - | - | 27.5 | V-1 |
| EP/PD-rGO5 | - | 4 | - | 28.0 | V-0 |
| EP/PD-rGO10 | - | - | 4 | 29.5 | V-1 |

**Table 2**

| Sample | C (at%) | O (at%) | N (at%) | P (at%) |
|---|---|---|---|---|
| GO | 68.9 | 31.1 | - | - |
| rGO | 74.0 | 18.4 | 7.6 | - |
| PD-rGO5 | 77.2 | 11.3 | 5.9 | 5.6 |
| PD-rGO10 | 76.9 | 11.7 | 6.0 | 5.4 |

**Table 3**

| Sample | $T_{-0.05}$ ($^oC$) | | $T_{max}$ ($^oC$) | | Char (700 °C, wt%) | |
|---|---|---|---|---|---|---|
| | $N_2$ | Air | $N_2$ | Air | $N_2$ | Air |
| EP | 360 | 371 | 378 | 391, 570 | 13.6 | 1.3 |
| EP/PiP-DOPO | 345 | 358 | 350 | 365, 565 | 14.7 | 2.4 |
| EP/PD-rGO5 | 343 | 358 | 353 | 366, 575 | 14.6 | 3.3 |
| EP/PD-rGO10 | 344 | 360 | 350 | 368, 572 | 15.3 | 2.5 |

**Table 4**

| Sample | PHRR (W/g) | THR (kJ/g) | $T_{PHRR}$ (%) |
|---|---|---|---|
| EP | 322 ± 12 | 28.1 ± 1.6 | 402 ± 2 |
| EP/PiP-DOPO | 256 ± 6 | 24.3 ± 1.4 | 386 ± 2 |
| EP/PD-rGO5 | 176 ± 8 | 22.8 ± 0.8 | 395 ± 3 |
| EP/PD-rGO10 | 157 ± 5 | 20.7 ± 1.1 | 394 ± 2 |

**Table 5**

| Sample | TTI (s) | PHRR ($kW/m^2$) | THR ($MJ/m^2$) | SPR ($m^2/s$) | Time to PHRR (s) | FIGRA ($kW/(m^2 \cdot s)$) |
|---|---|---|---|---|---|---|
| EP | 28 ± 1 | 1725 ± 33 | 78.2 ± 1.4 | 0.47 ± 0.05 | 54 ± 2 | 31.9 |
| EP/PiP-DOPO | 24 ± 2 | 1160 ± 15 | 54.4 ± 1.1 | 0.35 ± 0.04 | 50 ± 2 | 23.2 |
| EP/PD-rGO5 | 25 ± 1 | 1042 ± 27 | 49.3 ± 2.3 | 0.31 ± 0.03 | 52 ± 1 | 20.0 |
| EP/PD-rGO10 | 24 ± 2 | 821 ± 19 | 40.5 ± 1.9 | 0.32 ± 0.03 | 53 ± 3 | 15.5 |

**Table 6**

| Sample | Elastic modulus (GPa) | Tensile strength (MPa) | Elongation at break (%) |
|---|---|---|---|
| EP | 1.31 ± 0.13 | 50.6 ± 1.3 | 2.6 ± 0.3 |
| EP/PiP-DOPO | 1.26 ± 0.09 | 51.6 ± 0.9 | 3.4 ± 0.2 |
| EP/PD-rGO5 | 1.40 ± 0.07 | 51.8 ± 2.2 | 2.8 ± 0.5 |
| EP/PD-rGO10 | 1.45 ± 0.12 | 52.4 ± 1.6 | 2.5 ± 0.3 |

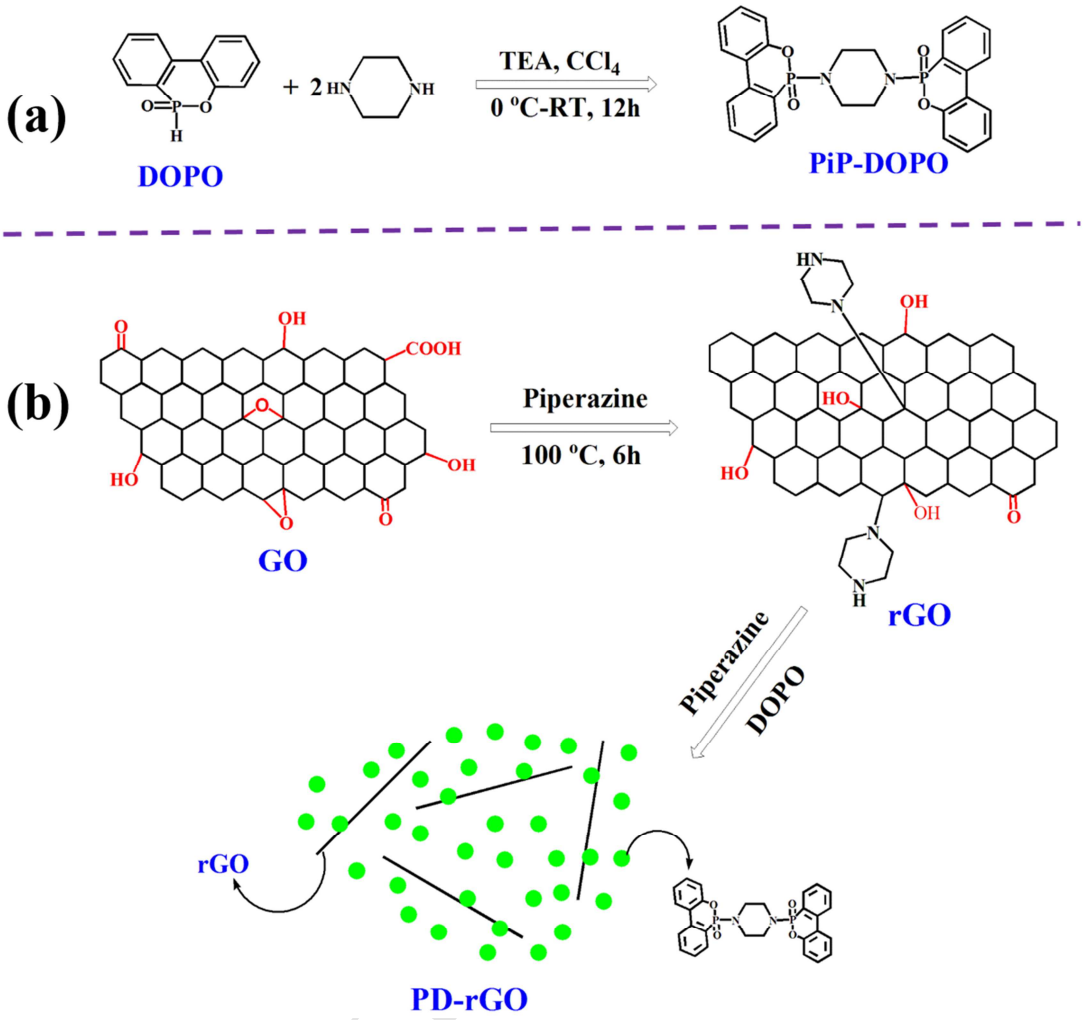


**Scheme 1**

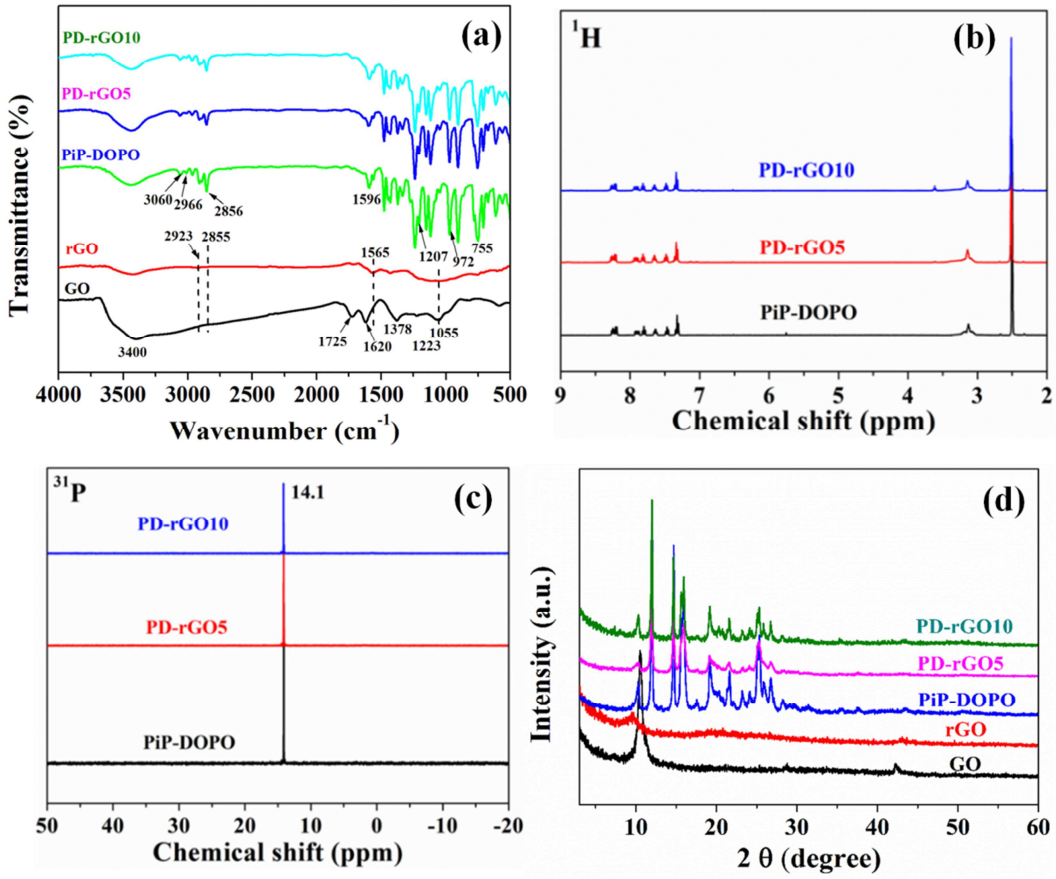


**Fig. 1**

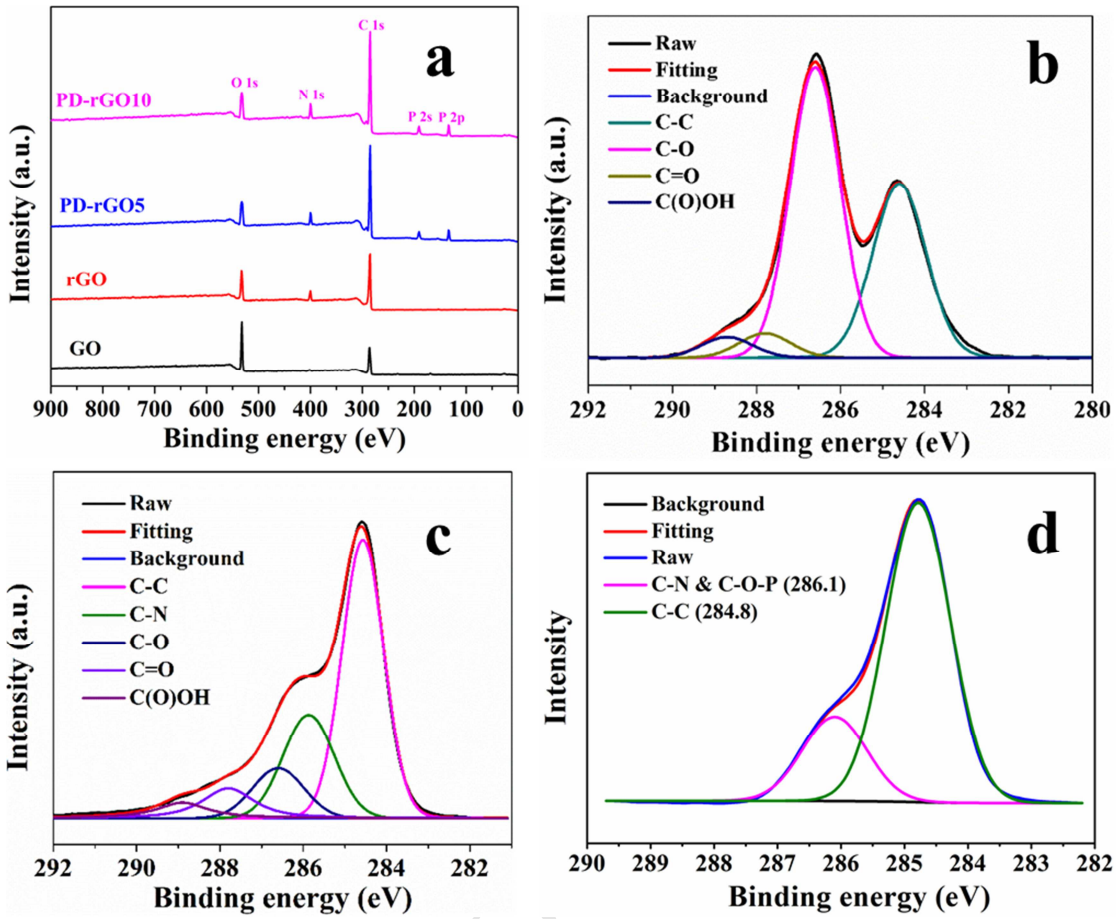


**Fig. 2**

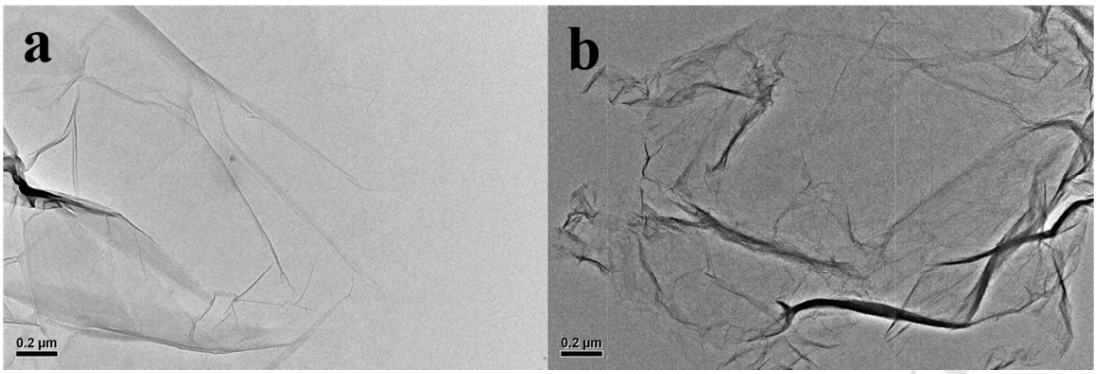


**Fig. 3**

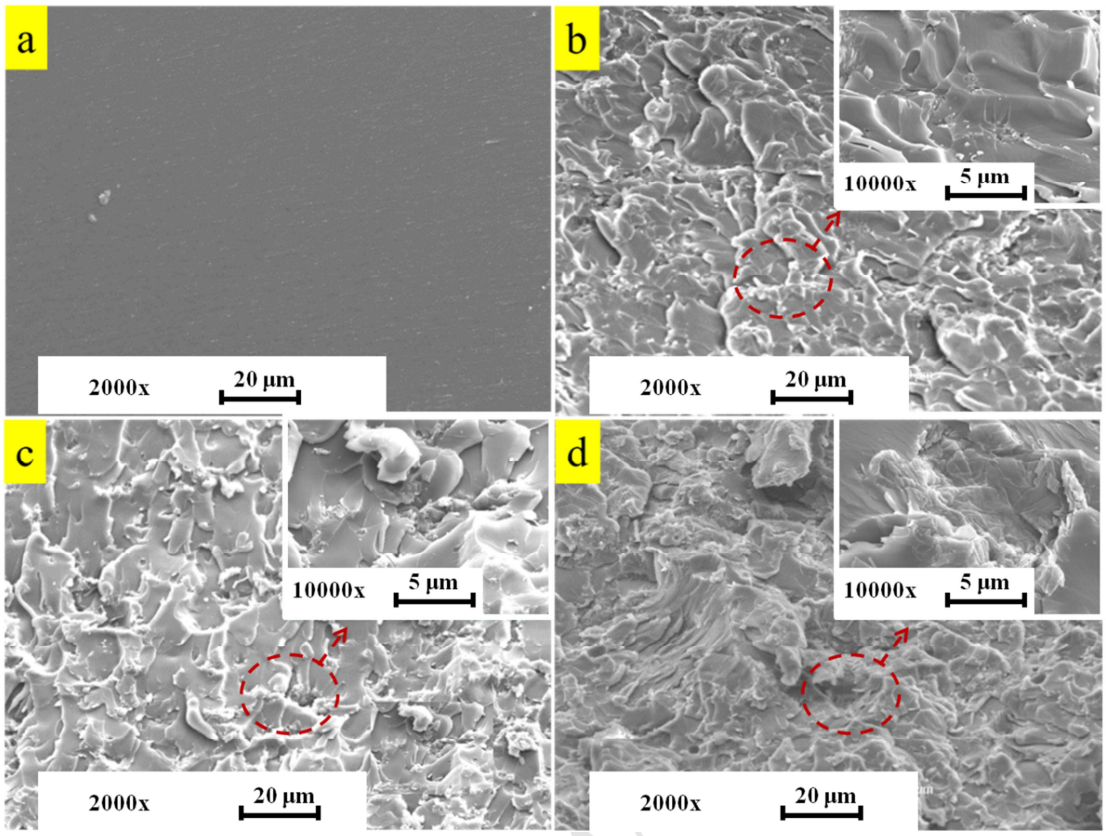


**Fig. 4**

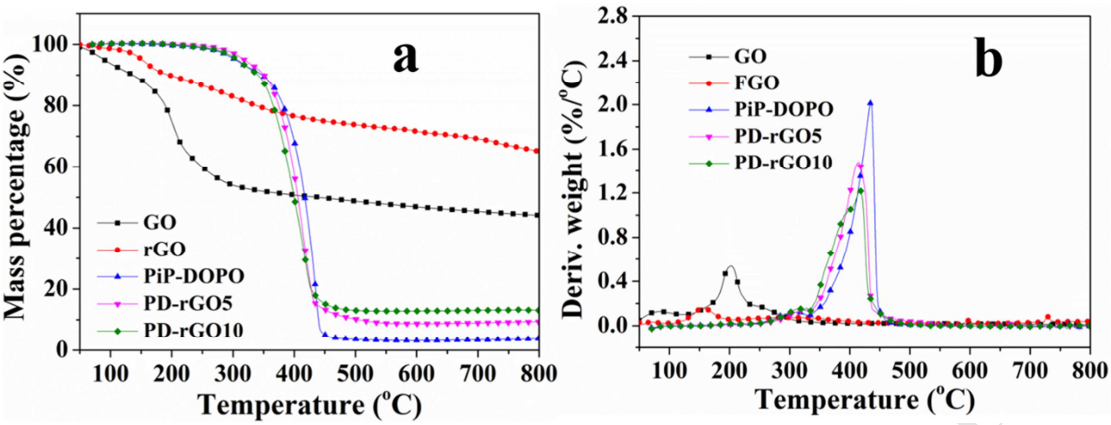


**Fig. 5**

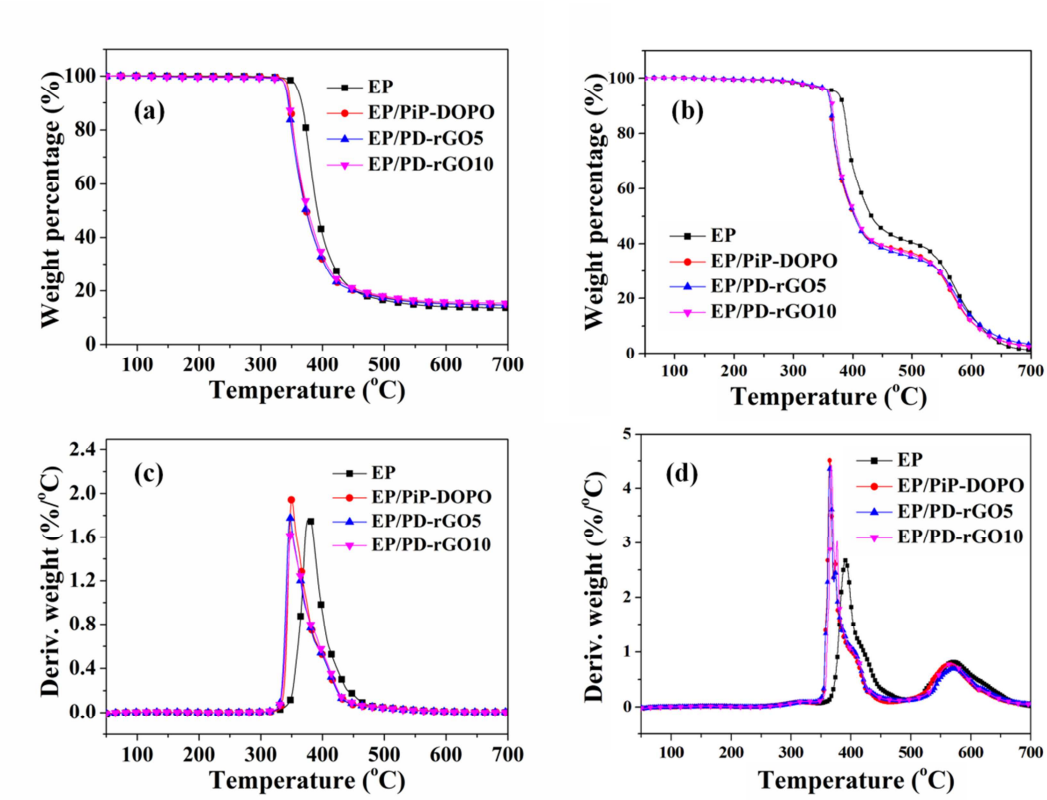


**Fig. 6**

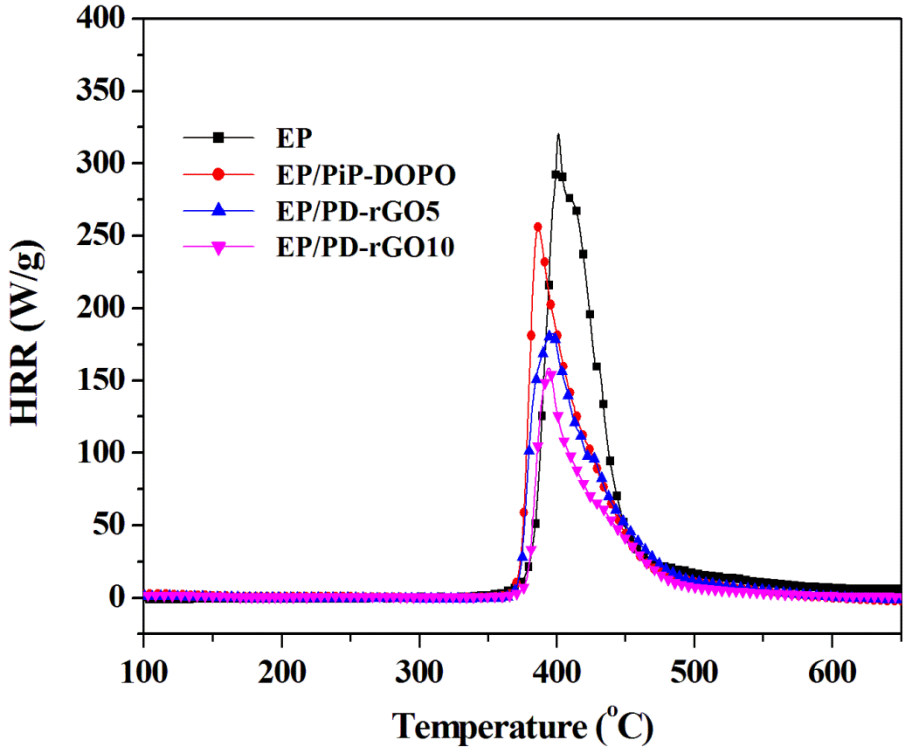


**Fig. 7**

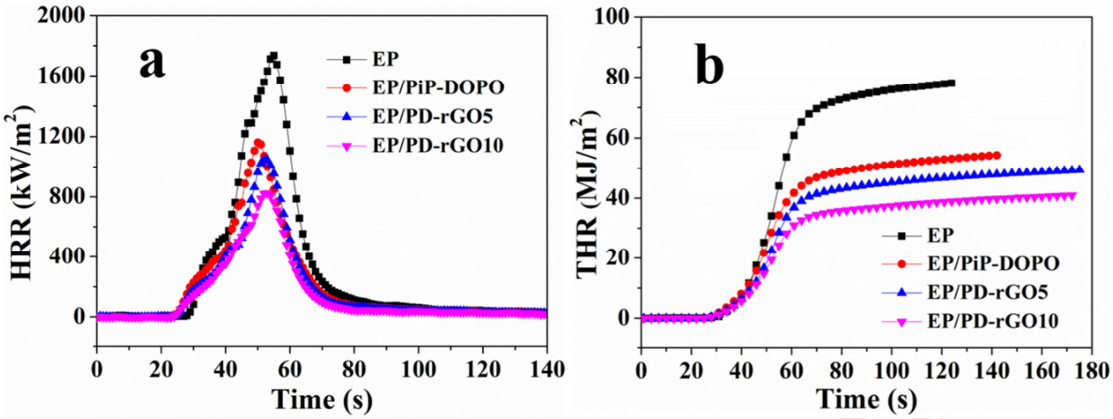


**Fig. 8**

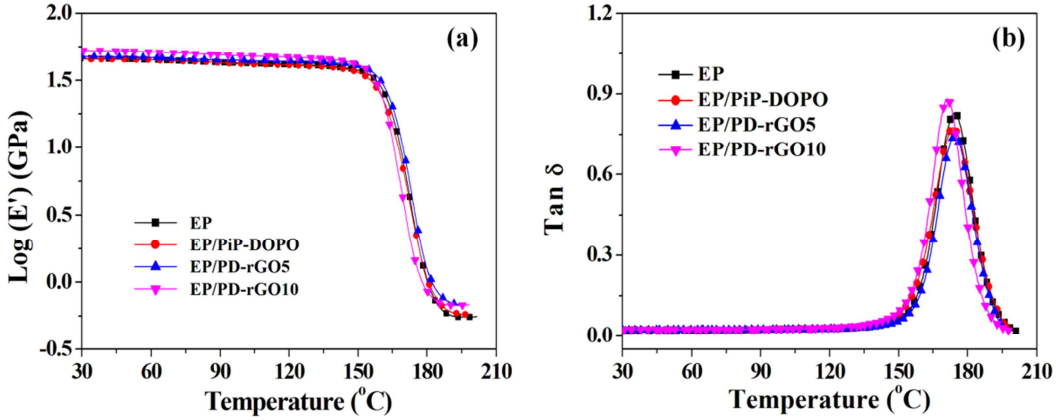


**Fig. 9**

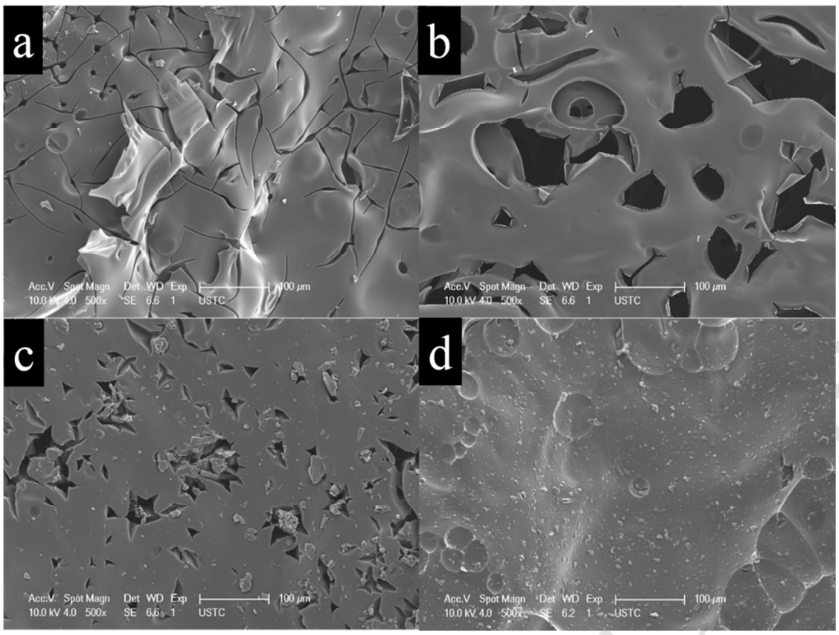


**Fig. 10**

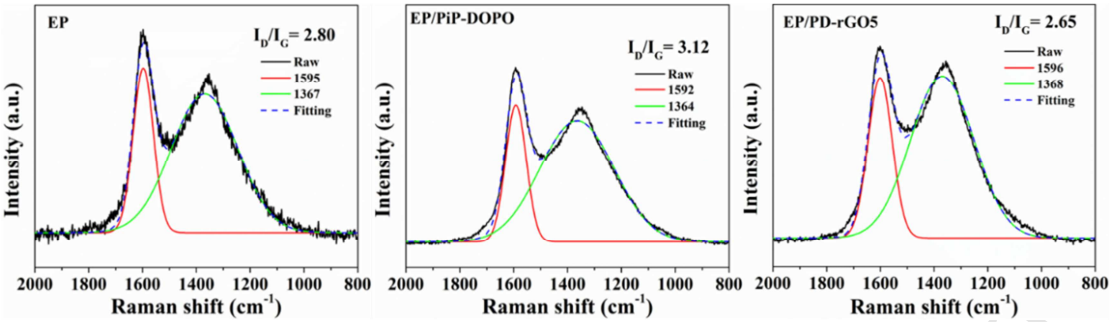


**Fig. 11**

# Highlights

1. Graphene oxide was reduced and modified by piperazine simultaneously using a one-pot method.

2. Reduced graphene oxide/DOPO-phosphonamidates hybrids were prepared by in situ reaction.

3. Remarkable enhancements on flame retardancy and mechanical properties of epoxy resin nanocomposites were achieved.

4. Enhancements mechanism was investigated with direct and detailed evidence.